RSC Sustainability

ROYAL SOCIETY OF CHEMISTRY

PAPER

View Article Online
View Journal | View Issue

Cite this: *RSC Sustainability*, 2024, **2**, 1859

Complexation-driven ion-exchange polymer inclusion membranes for separation of cobalt and nickel ions from lithium-ion *via* proton pumping†

Babafemi Adigun,[ab] Bishnu P. Thapaliya,*[c] Huimin Luo*[d] and Sheng Dai *[abc]

Cobalt and nickel are vital components of lithium-ion battery (LIB) cathodes; their increasing demand requires efficient recovery from spent LIBs to foster a sustainable battery future. The limitations of current separation technologies necessitate the development of more cost-effective, efficient, and eco-friendly metal recovery methods. Herein, we developed a complexation-driven ion-exchange polymer inclusion membrane (IEPIM) by confining an ionic liquid (IL) and a protic extractant in a polymer host to separate cobalt and nickel ions from lithium ions. While past studies achieved selective separation of cobalt ions using basic extractants in aqueous chloride solutions, this study utilizes a protic extractant to achieve a multi-ion separation in aqueous solution. Our approach relies on proton pumping facilitated by the protic extractant, making the separation process effective while avoiding harmful organic solvents. The IEPIM made from 50% PVDF-HFP (poly(vinylidene fluoride-*co*-hexafluoropropylene)) as the polymer host, 30% Cyanex 301 (bis(2,4,4-trimethylpentyl) dithiophosphinic acid) as the protic extractant, and 20% [C_8mim][NTf_2] (1-octyl-3-methylimidazolium bis(trifluoromethanesulfonyl)imide) as the plasticizer, efficiently separates Co^{2+} and Ni^{2+} from Li^+ in aqueous solution, with over 90% transport efficiency for Co^{2+} and 73% for Ni^{2+}. The membrane maintained this efficiency through three cycles, indicating its stability. These results demonstrate that the IEPIM could be a viable alternative to conventional metal ion separation methods, offering an environmentally sustainable and cost-effective strategy for recycling critical metals from spent lithium-ion batteries with the potential for industrial application in separation technology.

Received 6th February 2024
Accepted 13th May 2024

DOI: 10.1039/d4su00061g

rsc.li/rscsus

Sustainability spotlight

Sustainable recovery of metals from spent lithium-ion batteries (LIBs) is essential for mitigating the environmental and economic impacts of increasing cobalt and nickel demand. The inefficiencies, high energy demands, and toxic waste production of conventional recovery processes underscore the need for a sustainable, economically viable substitute. Our approach, utilizing Ion-Exchange Polymer Inclusion Membranes (IEPIMs) with a protic extractant, offers simultaneous separation of multiple ions in aqueous solutions, with impressive transport efficiencies exceeding 90% for cobalt and 73% for nickel. This innovation aligns with the UN's Sustainable Development Goals, particularly SDG 12 (Responsible Consumption and Production) and SDG 13 (Climate action), revolutionizing critical metal recycling, enhancing resource efficiency, and promoting a circular economy in the battery sector. Our work mitigates the environmental impact of e-waste and lowers the carbon footprint of metal extraction and processing, contributing to a sustainable, effective battery recycling infrastructure.

1. Introduction

The recovery of metals from waste, especially from expended LIBs, is critical for maintaining metal sustainability and environmental safety.[1,2] The demand for cobalt and nickel, key elements in LIB cathodes, has skyrocketed with the growth of the portable electronics and electric vehicle industries. This increase in demand poses challenges to their supply chains and has an environmental impact.[3–9] Conventional metal recovery methods, such as solvent extraction,[10,11] adsorption,[12,13] ion exchange,[14,15] and electrowinning,[16,17] come with significant drawbacks, including toxic waste creation, high costs, energy demands, and the need for large amounts of extractants. Therefore, there's a pressing need for an eco-friendly, efficient, and less extractant-dependent separation method to lessen environmental impact.

Polymer Inclusion Membranes (PIMs) provide a novel and continuous alternative to traditional metal separation

[a]*Department of Chemistry, The University of Tennessee, Knoxville, Tennessee 37996, USA*

[b]*Institute of Advanced Materials & Manufacturing, Knoxville, Tennessee 37920, USA*

[c]*Chemical Sciences Division, Oak Ridge National Laboratory, Oak Ridge, Tennessee 37831, USA. E-mail: prasadthapab@ornl.gov; dais@ornl.gov*

[d]*Manufacturing Science Division, Oak Ridge National Laboratory, Oak Ridge, Tennessee 37831, USA. E-mail: luoh@ornl.gov*

† Electronic supplementary information (ESI) available. See DOI: https://doi.org/10.1039/d4su00061g

techniques, offering efficiency and resource conservation. These membranes employ a selective approach, using a polymeric membrane infused with a specific extractant and a plasticizer to extract target metals from complex mixtures, like those found in spent battery leachates.[18,19] This method facilitates the selective transport of targeted metal ions, such as cobalt and nickel from complex mixtures, streamlining the process by combining extraction and stripping into one step. This reduces the need for extra separation phases, reduces extractant use, and minimizes environmental impact.[20,21]

PIMs have successfully recovered different metals; the key elements of PIMs—the polymer host, the extractant, and the plasticizer are essential for the membrane's effectiveness, stability, and ability to transport materials. The polymer host, typically cellulose triacetate (CTA)[22–24] or poly(vinyl chloride) (PVC),[25,26] forms the membrane's structure and determines its physical and chemical attributes. Poly(vinylidene fluoride-*co*-hexafluoropropylene) (PVDF-HFP), though less common, offers notable advantages such as strong chemical resistance and high stability. The extractant is crucial in PIM-based metal ion transport, as it binds and carries the target metal through the membrane. Various extractants are utilized, including bis(2,4,4-trimethylpentyl) phosphinic acid (Cyanex 272), 2-ethylhexyl phosphoric acid mono-2-ethylhexyl ester (PC-88A), di(2-ethylhexyl)phosphoric acid (D2EHPA), and *N*,*N*-dioctyl-1-octanamine (Alamine 336).[27–29] The plasticizer contributes to the membrane's effectiveness by lessening the intermolecular forces of the polymer, which increases flexibility and permeability for better metal ion transport.[18,19] Common plasticizers include 2-nitrophenyl octyl ether (2-NPOE),[30,31] *o*-nitrophenyl pentyl ether (ONPPE),[32,33] and tris(2-ethylhexyl) phosphate (TEHP).[34,35] PIMs have been effectively used in the recovery of various metals. For instance, Fajar *et al.* successfully applied PIM for extracting platinum (Pt), palladium (Pd), and rhodium (Rh) from the leachate of spent automotive catalysts using the ionic liquid trioctyl(dodecyl) phosphonium chloride ($P_{88812}Cl$). Over 90% recovery of Pt and Pd with high purity was achieved.[36] Several other studies have concentrated on selectively separating metals from used batteries. In one such study, Pospiech employed PIM to differentiate cobalt from nickel and lithium in a chloride solution, using trisooctylamine (TIOA) as the extractant. This process transported 74.5% of Co(II) ions into the receiving solution within 24 hours.[37] Recently, ionic liquids (ILs) have gained recognition as efficient ionic liquid plasticizers (ILPs) in PIMs, attributed to their structural resemblance to conventional plasticizers and their unique non-volatile nature.[38,39] Guo *et al.*, utilized ILs, specifically [$C_n$mim][PF_6], as plasticizers in the transport of (Cr(VI)). It was found that these IL plasticizers enhanced the membrane's permeability coefficient, thereby improving Cr(VI) transport.[27]

Herein, we aim to address the challenges of the traditional separation process by eliminating the need for toxic organic solvents using an IEPIM. The IEPIM, composed of a polymer host (PVDF-HFP), an extractant (Cyanex 301), and a plasticizer ([C_8mim][NTf_2]), is designed to separate cobalt and nickel ions from lithium ions in aqueous solutions. The separation strategy is based on proton pumping, driven by the pH gradient between the feed and stripping solutions, and facilitates the metal ion transport through the membrane. Previous studies have successfully extracted cobalt ions using basic extractants in chloride-based aqueous solutions; however, our strategy involves using a protic extractant to separate multiple ions at once in an aqueous solution with the potential for further individual separation. The IEPIM effectively separates cobalt and nickel from lithium ions in aqueous media, achieving a remarkable transport efficiency exceeding 90% for cobalt and 73% for nickel. The IEPIM maintains this efficiency effectively across three successive cycles, showing good stability over successive use and potential for industrial applications. Our study is focused on creating an environmentally sustainable method for metal separation and recovery, aiming to reduce the environmental impact of conventional separation processes.

2. Materials and methods

2.1 Materials

Poly(vinylidene fluoride-*co*-hexafluoropropylene) (PVDF-HFP, $M_w \sim 400\,000$, $M_n \sim 130\,000$, Sigma-Aldrich), bis(2,4,4-trimethylpentyl) dithiophosphinic acid (Cyanex 301, Solvay), acetone ($(CH_3)_2CO$, 99.5%, Fisher Chemical Company), lithium chloride (LiCl, 98.5%, Fisher Chemical Company), hydrochloric acid (HCl, 36%, Fisher Chemical Company), cobalt(II) chloride ($CoCl_2 \cdot 6H_2O$, 98%, Alfa Aesar), nickel(II) chloride ($NiCl_2 \cdot 6H_2O$, 98%, J. T. Baker Chemical Company) were used as received. 1-Octyl-3-methylimidazolium bis(trifluoromethanesulfonyl)imide ([C_8mim][NTf_2]) was synthesized by modified procedure from literature[40] (Fig. 1).

2.2 Membrane preparation

The pure PVDF-HFP membrane was prepared by dissolving PVDF-HFP pellets in acetone, stirring overnight, and casting the solution onto a Petri dish. Then, the solvent was evaporated to get the membrane used as a reference material for comparative analysis. The IEPIM membrane was prepared by dissolving PVDF-HFP, Cyanex 301, and [C_8mim][NTf_2] in 5 : 3 : 2 ratio by mass with a total weight of 0.2–0.3 g in acetone. The solution was stirred overnight at 25 ± 0.6 °C to form a homogenous solution and then poured into a 6.5 cm diameter Petri dish. The solvent was evaporated slowly over 24 hours, forming a membrane. The IEPIM membrane had a thickness of 45 ± 8

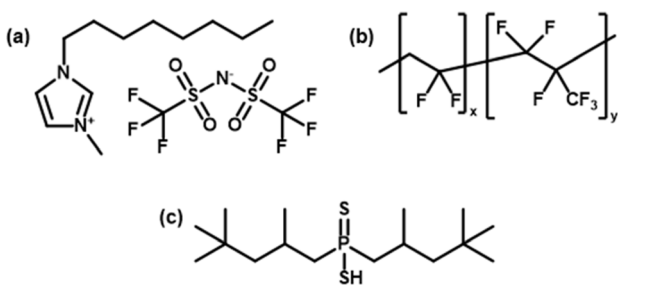

Fig. 1 Chemical structures (a) [C_8mim][NTf_2], (b) PVDF-HFP, (c) Cyanex 301.

μm, as measured with a digital calliper (Mitutoyo 293-832-30 micrometer).

2.3 Extraction and stripping experiments

0.2 g of IEPIM was immersed in 30 mL of 1 mM Co^{2+} and Ni^{2+} solution and shaken at 200 rpm on an orbital shaker at 25 °C for 24 hours. 1 mL sample was periodically taken out for analysis and replaced with an equal amount of the original solution to keep the volume constant. The concentration of the metal ions in the solution was measured before and after the extraction by inductively coupled plasma optical emission spectroscopy (ICP-OES) (Agilent 5110). The extraction efficiency (E%) was calculated using eqn (1) below.[28]

$$E(\%) = \frac{C_0^{\mathrm{f}} - C_t^{\mathrm{f}}}{C_0^{\mathrm{f}}} \times 100 \quad (1)$$

where 't' is the time (hours), the concentration of the metal ion in the feed solution at $t = 0$ (before extraction), at $t > 0$ (time of extraction) are denoted by C_0^{f} and C_t^{f} respectively.

Subsequently, the metal loaded IEPIM underwent a stripping process. It was placed in 30 mL of 2 M HCl for another 24 hours. Like the extraction phase, 1 mL aliquots were regularly taken from the solution and replaced by an equal volume of the fresh solution to maintain the volume. The concentration of the metal ions in the stripping solution was measured by ICP-OES. The stripping efficiency (S%) was calculated with eqn (2) below.[28]

$$S(\%) = \frac{C_0^{\mathrm{r}}}{C_{\mathrm{IEPIM}}} \times 100 \quad (2)$$

where 't' is time (hours), the concentration of the metal ion in the stripping solution at time $t > 0$ (the time of stripping) is denoted by C_0^{r}. The concentration of metal ions extracted into the membrane from the extraction experiment is denoted by C_{IEPIM}.

2.4 Mass loss of IEPIM

Two IEPIMs with a mass of 0.3102 ± 0.0003 g were immersed in 50 mL of deionized water and left for 24 hours at room temperature. After 24 hours, they were removed from the solution, cleaned, dried in the oven for more than 24 hours at 50 °C, and weighed. The process was repeated for three cycles. The solution was analyzed using a UV-Vis spectrometer and ICP-OES.

2.5 Transport experiments

The transport experiments involving the IEPIM were carried out using a jacketed glass compartment system. In this setup, the IEPIM was carefully placed between the compartments to ensure contact with the feed and stripping solutions. The surface area in contact with the feed and stripping solutions is 3.14×10^{-4} m^2 (diameter 20 mm). The feed (100 mL of 0.1 mM Co^{2+}, Ni^{2+}, Li^{+}) and stripping (100 mL of 2 M HCl) solutions were stirred at 700 rpm using magnetic stir bars. 1 mL aliquots were extracted from the solution, and an equal volume of the original solution was added to maintain the volume. The concentration of the metal ions in the solution was measured before and after the extraction by ICP-OES. The kinetics of the transport experiment is described by eqn (3); the rate constant k (h^{-1}), initial flux J_0 (mol m^{-2} s^{-1}), permeability coefficient P (m h^{-1}) and the transport efficiency TE (%) were calculated using the following equations.[28]

$$\ln\left(\frac{C_t^{\mathrm{f}}}{C_0^{\mathrm{f}}}\right) = -kt \quad (3)$$

$$P = \left(\frac{V}{A}\right)k \quad (4)$$

$$J_0 = P \cdot C_0^{\mathrm{f}} \quad (5)$$

$$\mathrm{TE}(\%) = \frac{C_t^{\mathrm{r}}}{C_t^{\mathrm{f}}} \times 100 \quad (6)$$

where C_0^{f} is the concentration of the metal ions (mol L^{-1}) in the feed solution at $t = 0$, C_0^{r} is the concentration of the metal ions (mol L^{-1}) in the stripping solution at $t > 0$ (stripping time), V is the volume (m^3) of the feed solution, A is the surface area (m^2) of the IEPIM in contact with the solutions.

3. Results and discussion

3.1 Membrane characterization

The surface morphology of the pure PVDF-HFP and IEPIM membranes was investigated using scanning electron microscopy (SEM), as shown in Fig. 2. The SEM image of the pure PVDF membrane displayed a dense and rough surface characterized by small, unevenly distributed pores (Fig. 2a). This morphology is likely due to solvent evaporation during membrane formation, which causes the development of these non-uniform pores. Upon incorporation of the extractant and plasticizer in fabricating the IEPIM, it was noted that the micropores became significantly filled (Fig. 2b). This is presumed to arise from the penetration of the extractant and plasticizer into the pores.

Before and after the transport experiments, the thermal analysis of pure PVDF-HFP and the IEPIM was examined. Thermogravimetric analysis (TGA) of pure PVDF-HFP, Cyanex 301, IEPIM before and after the transport experiments was examined as shown in Fig. 2c. Pure PVDF-HFP and Cyanex 301 each exhibit a single-step thermal decomposition at approximately 480 °C and 150 °C, respectively. However, the IEPIM undergoes a two-step decomposition, starting at around 150 °C due to the decomposition of the extractant and correlating with its proportion in the IEPIM, while the PVDF-HFP component continues to decompose at the same 480 °C. These observations indicate that the IEPIM's thermal stability is maintained up to 150 °C. The thermogravimetric analysis (TGA) of the IEPIM, conducted both before and after the extraction process was consistent, indicating that no residual metal ions remained in the membrane following the transport experiments. This finding confirms the membrane's efficiency in metal ion release during the transport process, highlighting its reusability without ion accumulation.

Fourier Transform Infrared (FTIR) spectroscopy was employed to identify the functional groups in the pure PVDF-HFP, Cyanex 301, and the IEPIM, covering a spectral range of

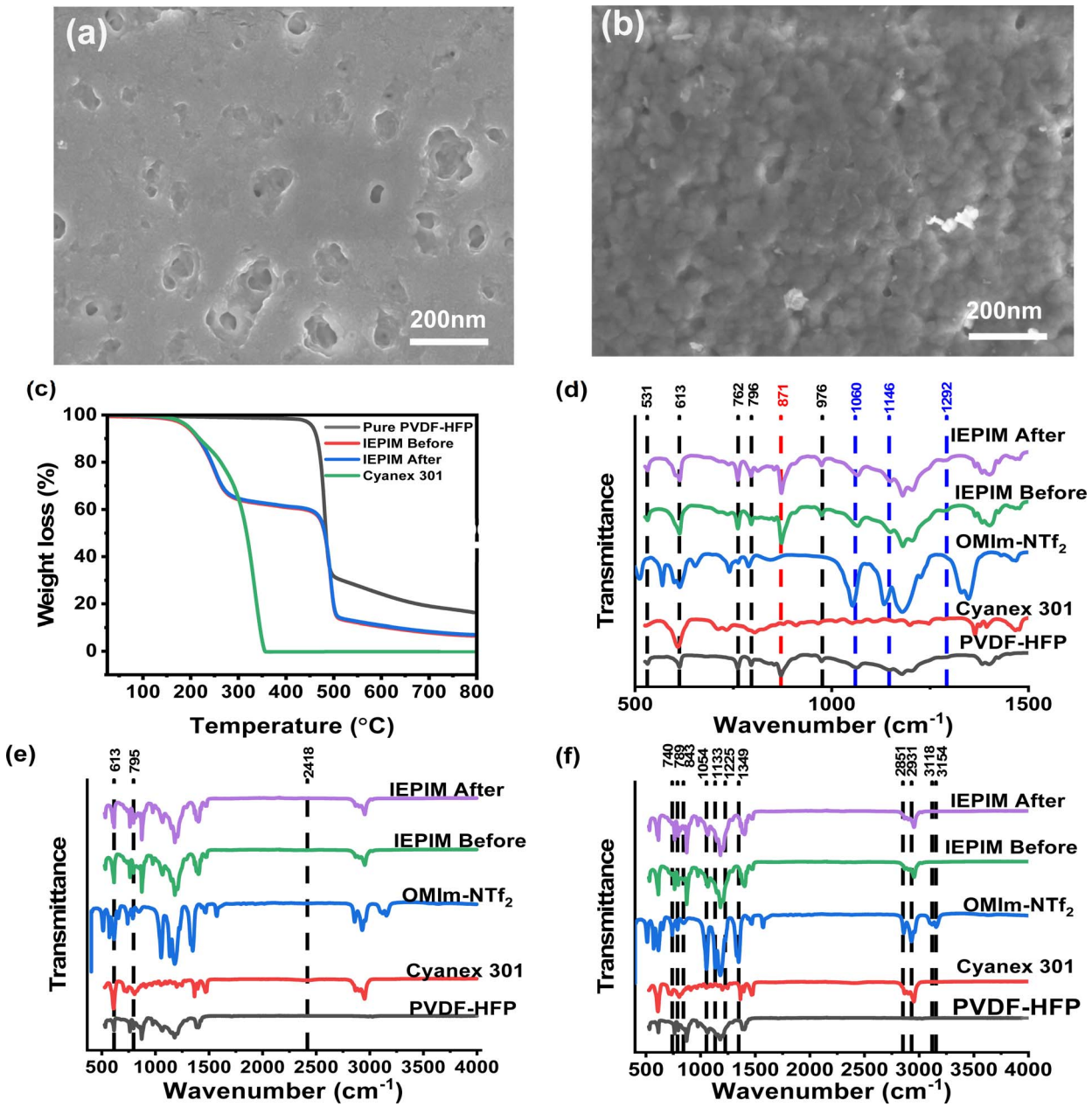

Fig. 2 Top view SEM image of (a) pure PVDF-HFP membrane and (b) IEPIM, (c) thermogravimetric analysis of pure PVDF-HFP, Cyanex 301, IEPIM before, and after transport experiments. FTIR spectra of pure PVDF-HFP membrane, Cyanex 301 [C_8mim][NTf_2] and IEPIM before and after use showing distinct peaks for (d) PVDF-HFP (e) Cyanex 301, and (f) [C_8mim][NTf_2].

500 to 4000 cm^{-1}. In Fig. 2d, distinctive peaks were observed, signifying both the crystalline and amorphous phases of the polymer in the FTIR spectra. Precisely, resonances at 531, 613, 762, 796, and 976 cm^{-1} correspond to the α-phase crystalline regions, while the peak at 871 cm^{-1} aligns with the amorphous phase of the polymer. Additional vibrational modes at 1060, 1146, and 1292 cm^{-1} can be attributed to the symmetric stretching of –CF groups, the stretching of $–CF_2$ moieties, and the symmetric stretching of $–CF_3$ bonds, respectively. In the FTIR spectra of Cyanex 301, major peaks are discerned at 613, 795, and 2418 cm^{-1}, corresponding to stretching bonds associated with P═S, S═P–SH, and S–H functionalities, respectively, as shown in Fig. 2e. Although the 2418 cm^{-1} peak was less discernible in the combined spectra, its individual plotting (Fig. S1†) made it more apparent.[41–44]

Similarly, the FTIR spectra of [C_8mim][NTf_2], as shown in Fig. 2f, exhibits peaks at 740, 789, 843, 1054, 1133, 1225, 1349 cm^{-1} which correspond to the symmetric bending of CF_3, C–S & S–N stretching, in-plane bending C–H peak of imidazolium ring, S–N–S asymmetric stretching, symmetric stretching of CF_3; stretching of C–N within the imidazole ring and asymmetric deformation vibrations of SO_2 bonds, respectively. Peaks at 2859–2931 cm^{-1} correspond to the aliphatic stretching of C–H, and 3118–3154 cm^{-1} correspond to the C–H stretching

specific to the imidazole ring.[45] The IEPIM membrane's FTIR spectra showed the distinct peaks of its constituent materials, confirming their successful incorporation. Notably, the absence of specific peaks (3118–3154 cm^{-1}) in the IEPIM's spectra suggested possible inhibitions in the imidazole ring's vibrations after the membrane formation. Furthermore, no significant spectral changes were observed in the IEPIM membrane before and after metal ion transport, indicating the structural stability of the membrane throughout the process.

3.2 Extraction and stripping studies with cobalt(II) and nickel(II)

The IEPIM was immersed in 30 mL of 1 mM Co^{2+} and Ni^{2+} solutions for 8 hours. The normalized concentrations of Co^{2+} and Ni^{2+} in the feed solution are shown in Fig. 3a. The Co^{2+} and Ni^{2+} concentrations rapidly reduced in the first 2 hours and reached equilibrium around 8 hours, after which the concentrations no longer decreased significantly. The IEPIM extracted 98% of Co^{2+} and 91% of Ni^{2+} in the feed solutions in 8 hours. The equation below (eqn (7)) describes the extraction mechanism of Co^{2+} and Ni^{2+} in solvent extraction studies with Cyanex 301 as the extractant. The mechanism involves a cationic exchange between the H^+ and the metal ions, extracted by exchanging two protons with the extractant.

$$M_{(aq)}{}^{2+} + 2HA_{(mem)} \leftrightharpoons MA_{2(mem)} + 2H_{(aq)}{}^{+} \quad (7)$$

where "aq" and "mem" represent the aqueous and membrane phases, respectively, it was assumed that the extraction mechanism in solvent extraction is the same in the IEPIM system.

A 2 M HCl solution was employed as the stripping solution for the stripping phase. This process, guided by the exact mechanism (eqn (7)), resulted in the stripping of significant amounts of Co^{2+} and Ni^{2+} from the IEPIM, as shown in Fig. 3b. However, complete stripping of the metal ions was not achieved. Over 24 hours, the IEPIM stripped 90% of Co^{2+} and 79% of Ni^{2+}.

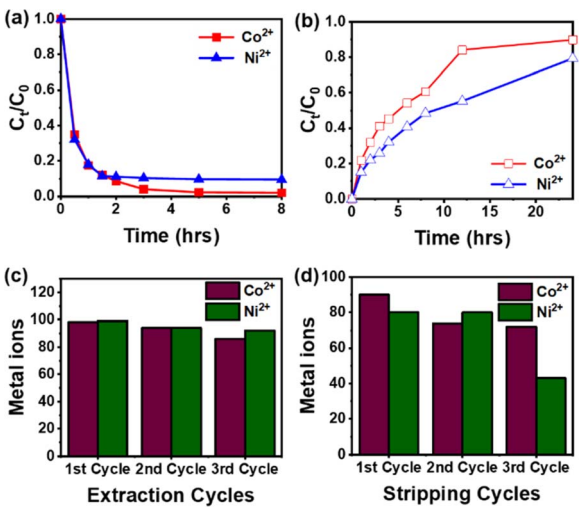

Fig. 3 (a) Extraction of Co^{2+} and Ni^{2+} into IEPIM in the feed solutions. (b) Stripping of Co^{2+} and Ni^{2+} from IEPIM in the stripping solutions. Three cycles of (c) extraction of Co^{2+} and Ni^{2+} into IEPIM and (d) stripping Co^{2+} and Ni^{2+} from IEPIM.

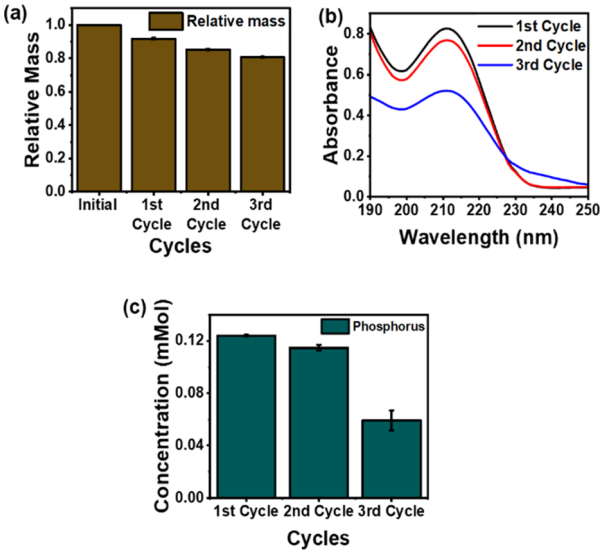

Fig. 4 (a) Mass changes of IEPIM for three cycles (b) UV-Vis spectra showing imidazolium peaks (c) phosphorus concentration in the solution after immersion in deionized water.

After three cycles, there was a noticeable decrease in extraction efficiency for Co^{2+}; the extraction efficiency decreased from an initial 98% to 86%, while the stripping efficiency declined from 90% to 72%. In contrast, for Ni^{2+}, the extraction performance remained consistent, exceeding 90% after each cycle, while the stripping efficiency significantly declined from 80% to 43% (Fig. 3c and d). This decline in performance is likely due to the loss of the extractant during the processes.

The performance drop of the IEPIM was investigated by evaluating its mass changes. The IEPIM was immersed in deionized water for 24 hours. Fig. 4a shows the relative mass of the IEPIM after each cycle, where the relative mass is calculated as the ratio of the mass of the IEPIM after immersion (m) to the initial mass of the IEPIM (m_0). A notable mass loss of approximately 8% was observed following each cycle. To investigate the leakage of extractant and IL, analyses were conducted on the solution after each cycle using UV-Vis and ICP-OES. The UV-Vis spectra, depicted in Fig. 4b, exhibit a characteristic peak at 211 nm corresponding to the imidazolium ring in C_8mim-NTf_2. Additionally, Fig. 4c displays the phosphorus content in the solution after each cycle, with a decrease in phosphorus concentration mirroring the trend seen in the UV-Vis spectra of the imidazolium ring. These observations indicate that the mass loss in the IEPIM is due to the leakage of extractant and IL from the membrane.

3.3 Membrane transport of Co(II) and Ni(II) and separation from Li(I)

The transport experiments utilized an IEPIM membrane in a system designed to separate Co^{2+} and Ni^{2+} from Li^+. This system enabled concurrent extraction and stripping of these metal ions from the feed to the stripping solution. The

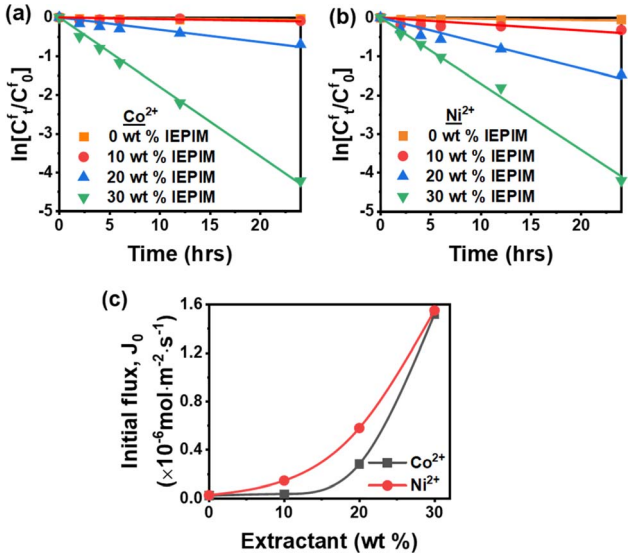

Fig. 5 Kinetic plots of the (a) transport of Co^{2+}, (b) transport of Ni^{2+}, and (c) initial flux at varying weight composition of the extractant across IEPIM in the feed solution.

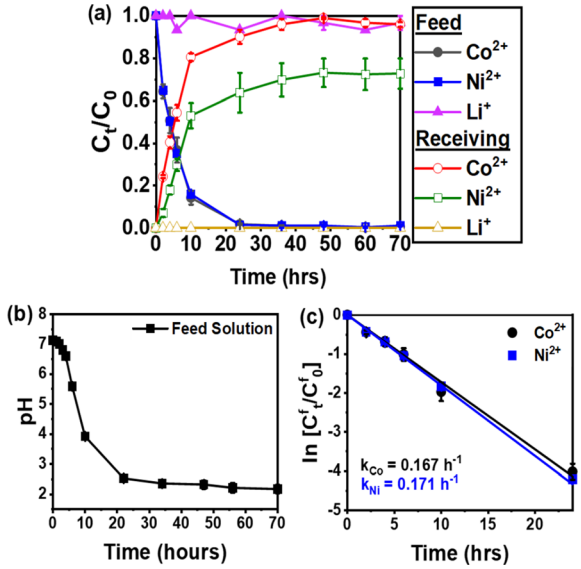

Fig. 6 (a) Transport of Co^{2+} and Ni^{2+} across an IEPIM in the feed and stripping solutions over time (b) plot of pH in the feed solution over time (c) kinetic plots of the transport of Co^{2+} and Ni^{2+} across the IEPIM in the feed solution.

extractant plays a significant role in facilitating the transport of ions across the IEPIM. Therefore, the effect of the extractant's concentration in the IEPIM was studied in the transport of Co^{2+} and Ni^{2+} across the IEPIM. The weight percent composition of the IEPIM varied from 0% to 30% by weight (Fig. S2†). In the experiments, a feed solution containing 0.1 mM of Li^+, Co^{2+}, and Ni^{2+} and a 2 M HCl as the receiving solution. The rate constants (k) and the initial flux (J_0) of Co^{2+} and Ni^{2+} increased with an increasing extractant concentration (wt% composition), as shown in Fig. 5a–c. The kinetic parameters of the transport of Co^{2+} and Ni^{2+} across the IEPIMs are summarized in Table 1. The most effective transport was observed with the 30 wt% composition IEPIM, demonstrating the highest flux values with a flux of 1.58 and 1.51 μmol m^{-2} s^{-1} for Co^{2+} and Ni^{2+}, respectively. However, no transport of Li^+ ions was observed across the membranes. These findings demonstrated that the extractant facilitates the transport of the ions, even at low concentrations. The optimal concentration for effective ion transport was established at 30 wt% of the extractant and was used for the transport experiments in this work.

Fig. 6a shows the successful transport of Co^{2+} and Ni^{2+} across the IEPIM, with a corresponding decrease in these ions in the feed solution and an increase in the stripping solution. At the same time, Li^+ remained predominantly in the feed solution. After 70 hours, the IEPIM achieved a transport efficiency of 96% for Co^{2+} and 73% for Ni^{2+} while 96% of Li^+ ions remained in the feed solution.

The pH of the feed solution decreases over time, indicating the diffusion of protons across the IEPIM from the stripping solution to the feed solution (Fig. 6b). This process suggests that metal ion transport occurs *via* a cation exchange mechanism facilitated by proton pumping. From the plot of In C_t^f/C_0^f In against time for the feed solution in Fig. 6c, the rate constant (k), permeability coefficient (P), and initial flux (J_0) were calculated using eqn (3)–(5). These values are listed in Table 2.

3.4 Effect of membrane thickness on transport of ions

The membrane's thickness is crucial in ion transport efficiency in the IEPIM. To investigate this, IEPIMs of identical

Table 1 Co^{2+} and Ni^{2+} rate constant (k), permeability coefficient (P), and initial fluxes (J_0) for transport across IEPIM with varying weight compositions

Extractant wt (%)	Metal ions	k (h^{-1})	P ($\times 10^{-6}$ m s^{-1})	J_0 ($\times 10^{-6}$ mol m^{-2} s^{-1})	Transport efficiency (%)
0	Co^{2+}	0.00267	0.236	0.0236	0
	Ni^{2+}	0.00305	0.270	0.0270	1
10	Co^{2+}	0.00419	0.370	0.370	12
	Ni^{2+}	0.0166	1.46	0.146	19
20	Co^{2+}	0.0319	2.82	0.282	94
	Ni^{2+}	0.0656	5.80	0.580	67
30	Co^{2+}	0.167	15.8	1.580	95
	Ni^2	0.171	15.1	1.510	70

Table 2 Co^{2+} and Ni^{2+} rate constant (k), permeability coefficient (P), and initial fluxes (J_0) for transport across IEPIM

Metal ions	k (h^{-1})	P ($\times 10^{-6}$ m s^{-1})	J_0 ($\times 10^{-6}$ mol m^{-2} s^{-1})	Transport efficiency (%)
Co^{2+}	0.167	14.8	1.48	96
Ni^{2+}	0.171	15.1	1.51	73

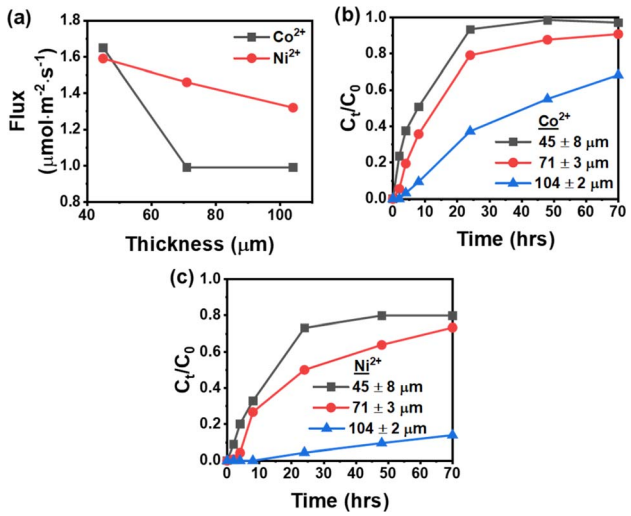

Fig. 7 (a) Initial flux of Co^{2+} and Ni^{2+} (b) transport efficiency of Co^{2+} (c) transport efficiency of Ni^{2+} at different membrane thicknesses across IEPIM.

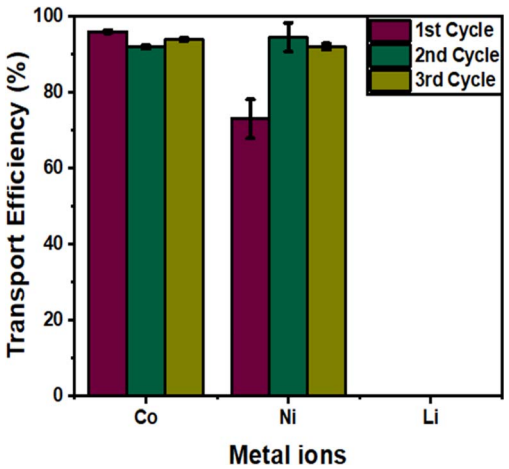

Fig. 8 Transport efficiency of 3 transport cycles. Feed solution: 100 mL of 0.1 mM Li^+, Co^{2+}, and Ni^{2+}. Receiving solution: 2 M HCl. Membrane composition 50% wt PVDF-*co*-HFP and 30% wt Cyanex 301 and 20% wt [C_8mim][NTf_2].

composition but varying thicknesses, ranging from 45 ± 8 μm to 104 ± 2 μm, were examined. Fig. 7a shows the initial flux of the ions across the IEPIM at different thicknesses. The initial flux of Ni^{2+} decreases linearly as the thickness of the IEPIM increases from 45–104 μm. However, for Co^{2+}, the initial flux reduces as the thickness increases from 45 μm to 71 μm and remains the same as the thickness increases from 71 to 104 μm.

Fig. 7b and c demonstrate the influence of membrane thickness on transport efficiency. Both Co^{2+} and Ni^{2+} transport efficiencies slightly decrease as the thickness increases from 45 to 71 μm, followed by a substantial drop from 71 to 104 μm, particularly for Ni^{2+}. In the transport involving the thickest version of the IEPIM (104 μm), a notable delay was observed in the ion transport process. The Co^{2+} ions were detected in the receiving solution after a 2 hours interval, whereas the appearance of Ni^{2+} ions required a significantly longer duration of 24 hours. This observed delay in ion transport could potentially be linked to the longer diffusion path necessitated by the increased thickness of the membrane. This finding highlights the membrane thickness's impact on ion transport efficiency in IEPIM systems.

3.5 Membrane stability

The stability of the IEPIM was evaluated through three consecutive cycles of use, as shown in Fig. 8, with both the feed and stripping solutions being replenished after each cycle.

The rate constant (k), permeability coefficient (P), and initial fluxes (J_0) for each transport cycle across IEPIM are summarized in Table 3. The transport efficiency of Co^{2+} remained above 90% for all three cycles. The transport efficiency of Ni^{2+} improved from 73% to 94% and 92% in the second and third cycles respectively while over 90% of Li^+ remained in the feed solution for the three cycles. However, the initial fluxes in the feed solution decreased after each cycle, as shown by the lower transport efficiency of both ions after 24 hours in Fig. S4.† The transport efficiency of Co^{2+} and Ni^{2+} after 24 hours was 90%, 50%, and 41% for Co^{2+}, and 64%, 54%, and 39% for Ni^{2+} for the first, second, and third cycles, respectively. The IEPIM showed higher selectivity for Co^{2+} over Ni^{2+} in the first cycle but no significant difference in the later cycles.

The IEPIM was further subjected to 5 cycles of use and subsequently characterized (Fig. S5–S7†). The thermal gravimetric analysis (TGA) of the IEPIM before and after 5 cycles showed that the general features of the IEPIM remained similar.

Elemental analysis using Energy Dispersive X-ray Fluorescence (EDXRF) before and after 5 cycles of transport experiments confirmed the presence of 1% of Co^{2+} and 3.6% of Ni^{2+}. The presence of the metal ions may have contributed to membrane fouling, leading to a decline in transport efficiency in the 4th and 5th cycles.

3.6 Mechanism

The potential transport mechanisms for cobalt and nickel ions through the IEPIM were deduced from their observed behaviors, as demonstrated in Fig. 9. Initially, Co^{2+} and Ni^{2+} ions present in the feed solution were extracted into the membrane

Table 3 Co^{2+} and Ni^{2+} rate constant (k), permeability coefficient (P), and initial fluxes (J_0) for transport across IEPIM for the three cycles

Cycle	Metal ions	k (h^{-1})	P ($\times 10^{-6}$ m s^{-1})	J_0 ($\times 10^{-6}$ mol m^{-2} s^{-1})	Transport efficiency (%)
1st	Co^{2+}	0.172	15.2	0.0236	96
	Ni^{2+}	0.176	15.5	0.0270	73
2nd	Co^{2+}	0.040	3.54	0.370	92
	Ni^{2+}	0.059	5.23	0.146	94
3rd	Co^{2+}	0.030	2.68	0.282	94
	Ni^{2+}	0.040	3.54	0.580	92

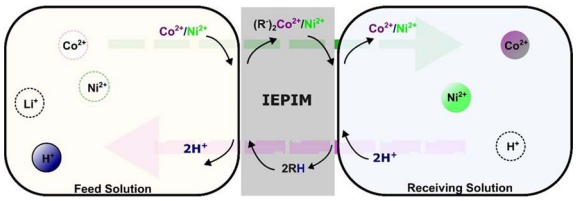

Fig. 9 Plausible mechanism for transporting Co^{2+} and Ni^{2+} across IEPIM in this study.

through ion exchange interactions with protons from the extractant at the interface between the feed solution and IEPIM and formed metal complexes with the extractant in the IEPIM. Subsequently, at the IEPIM-stripping solution interface, metal ions are released from these complexes and replaced by protons from the stripping solution, facilitated by proton pumping through the protic extractant. This mechanism enables the concurrent transport of Co^{2+} and Ni^{2+} from the feed solution while moving protons from the stripping to the feed solution. The extractant's affinity for Co^{2+} and Ni^{2+}, characterized as soft metal ions, is due to its nature as a soft ligand, leading to the selective transport of these ions over hard ions like Li^{+}. The high acid concentration in the stripping solution ensures continuous proton transfer, as indicated by the pH decrease in the feed solution.

4. Conclusions

In summary, we have successfully demonstrated the transport of cobalt and nickel ions from lithium ions in aqueous media by using an IEPIM composed of Cyanex 301 as an extractant, PVDF-HFP as the polymer host, and $[C_8mim][NTf_2]$ as the plasticizer. The transport of the metal ions is facilitated by proton pumping through protons from the protic extractant in exchange for the metal ions. This environmentally benign and cost-effective approach eliminates the requirement for volatile solvents. The developed IEPIM successfully demonstrated transport efficiency exceeding 90% for Co^{2+} and 74% for Ni^{2+}. Furthermore, the membrane maintained its efficiency over successive operational cycles, surpassing 90% for Co^{2+} across three cycles and Ni^{2+} showing 73% after the first cycle and 94% and 92% for the second and third cycles, respectively, indicating the membrane's stability. However, addressing potential concerns regarding the loss or leakage of extractant and ionic liquid is essential, which could be critical in practical extraction and back-extraction processes, warranting further investigation and optimization for real-world applications. These results underscore the IEPIM's potential as an appealing alternative to conventional metal ion separation methods. Successful integration on an industrial scale could revolutionize the separation landscape, promoting eco-friendliness, cost-effectiveness, and the efficient recycling of critical metal ions from spent LIBs.

Conflicts of interest

There are no conflicts to declare.

Acknowledgements

This research was performed through the Re-Cell Center, which gratefully acknowledges support from the U. S. Department of Energy (DOE), Office of Energy Efficiency and Renewable Energy, and the Vehicle Technologies Office. This manuscript has been authored in part by UT-Battelle, LLC, under contract DE-AC05-00OR22725 with the US Department of Energy (DOE). The US government retains and the publisher, by accepting the article for publication, acknowledges that the US government retains a nonexclusive, paid-up, irrevocable, worldwide license to publish or reproduce the published form of this manuscript, or allow others to do so, for US government purposes. DOE will provide public access to these results of federally sponsored research in accordance with the DOE Public Access Plan (**http://energy.gov/downloads/doe-public-access-plan**).

References

1 M. Henckens, P. Driessen and E. Worrell, *Resour., Conserv. Recycl.*, 2014, **93**, 1–8.
2 M. Reuter, C. Hudson, A. Van Schaik, K. Heiskanen, C. Meskers and C. Hagelüken, *A Report of the Working Group on the Global Metal Flows to the International Resource Panel*, 2013.
3 M. Li and J. Lu, *Science*, 2020, **367**, 979–980.
4 N. Nitta, F. Wu, J. T. Lee and G. Yushin, *Mater. Today*, 2015, **18**, 252–264.
5 M. S. Whittingham, *Chem. Rev.*, 2004, **104**, 4271–4302.
6 X. Zheng, Z. Zhu, X. Lin, Y. Zhang, Y. He, H. Cao and Z. Sun, *Engineering*, 2018, **4**, 361–370.
7 A. Mayyas, D. Steward and M. Mann, *Sustainable Mater. Technol.*, 2019, **19**, e00087.

8 E. A. Olivetti, G. Ceder, G. G. Gaustad and X. Fu, *Joule*, 2017, **1**, 229–243.
9 B. E. Murdock, K. E. Toghill and N. Tapia-Ruiz, *Adv. Energy Mater.*, 2021, **11**, 2102028.
10 W. Yoshida, F. Kubota, Y. Baba, S. D. Kolev and M. Goto, *ACS Omega*, 2019, **4**, 21122–21130.
11 X. Sun, H. Luo and S. Dai, *Talanta*, 2012, **90**, 132–137.
12 Y. A. Aydın and N. D. Aksoy, *Chem. Eng. J.*, 2009, **151**, 188–194.
13 S. Gupta and B. Babu, *Chem. Eng. J.*, 2009, **150**, 352–365.
14 A. B. Botelho Junior, D. B. Dreisinger and D. C. Espinosa, *Min., Metall., Explor.*, 2019, **36**, 199–213.
15 J.-c. Lee, H.-J. Hong, K. W. Chung and S. Kim, *Sep. Purif. Technol.*, 2020, **246**, 116896.
16 A. Fathima, J. Y. B. Tang, A. Giannis, I. Ilankoon and M. N. Chong, *Chemosphere*, 2022, **298**, 134340.
17 S. Hussaini and A. M. Tita, in *Recycling Technologies for Secondary Zn–Pb Resources*, Springer, 2023, pp. 403–459.
18 L. Nghiem, P. Mornane, I. Potter, J. Perera, R. Cattrall and S. Kolev, *J. Membr. Sci.*, 2006, **281**, 7–41.
19 M. I. G. S. Almeida, R. W. Cattrall and S. D. Kolev, *J. Membr. Sci.*, 2012, **415–416**, 9–23.
20 A. T. Fajar and M. Goto, *J. Chem. Eng. Jpn.*, 2023, **56**, 2153547.
21 B. Keskin, B. Zeytuncu-Gökoğlu and I. Koyuncu, *Chemosphere*, 2021, **279**, 130604.
22 A. Kaya, C. Onac, A. Surucu, E. Karapinar, H. K. Alpoguz and B. Tabakci, *J. Inclusion Phenom. Macrocyclic Chem.*, 2014, **79**, 103–111.
23 C. Cai, F. Yang, Z. Zhao, Q. Liao, R. Bai, W. Guo, P. Chen, Y. Zhang and H. Zhang, *J. Membr. Sci.*, 2019, **579**, 1–10.
24 O. Kebiche-Senhadji, L. Mansouri, S. Tingry, P. Seta and M. Benamor, *J. Membr. Sci.*, 2008, **310**, 438–445.
25 S. D. Kolev, Y. Baba, R. W. Cattrall, T. Tasaki, N. Pereira, J. M. Perera and G. W. Stevens, *Talanta*, 2009, **78**, 795–799.
26 N.-S. Abdul-Halim, P. G. Whitten and L. D. Nghiem, *Sep. Purif. Technol.*, 2013, **119**, 14–18.
27 L. Guo, Y. Liu, C. Zhang and J. Chen, *J. Membr. Sci.*, 2011, **372**, 314–321.
28 W. Yoshida, Y. Baba, F. Kubota, S. D. Kolev and M. Goto, *J. Membr. Sci.*, 2019, **572**, 291–299.
29 H. Dahdah, F. Sellami, S. Dekkouche, M. Benamor and O. Senhadji-Kebiche, *Polym. Bull.*, 2023, **80**, 6495–6525.
30 D. Wang, R. W. Cattrall, J. Li, M. I. G. Almeida, G. W. Stevens and S. D. Kolev, *J. Membr. Sci.*, 2017, **542**, 272–279.
31 D. Wang, J. Hu, Y. Li, M. Fu, D. Liu and Q. Chen, *J. Membr. Sci.*, 2016, **501**, 228–235.
32 E. Radzyminska-Lenarcik and M. Ulewicz, *Pol. J. Chem. Technol.*, 2015, **17**, 51–56.
33 B. Pospiech, *Arch. Metall. Mater.*, 2015, 2933–2938.
34 M. Monroy-Barreto, A. N. Bautista-Flores, N. M. Munguia Acevedo, E. R. de San Miguel and J. de Gyves, *Ind. Eng. Chem. Res.*, 2021, **60**, 3385–3396.
35 M. Macías and E. Rodríguez de San Miguel, *Water, Air, Soil Pollut.*, 2021, **232**, 1–16.
36 A. T. Fajar, T. Hanada, M. L. Firmansyah, F. Kubota and M. Goto, *ACS Sustain. Chem. Eng.*, 2020, **8**, 11283–11291.
37 B. Pospiech, *Physicochem. Probl. Miner. Process.*, 2022, **58**, 152997.
38 M. Rahman and C. S. Brazel, *Polym. Degrad. Stab.*, 2006, **91**, 3371–3382.
39 M. P. Scott, C. S. Brazel, M. G. Benton, J. W. Mays, J. D. Holbrey and R. D. Rogers, *Chem. Commun.*, 2002, 1370–1371.
40 P. Bonhote, A.-P. Dias, N. Papageorgiou, K. Kalyanasundaram and M. Grätzel, *Inorg. Chem.*, 1996, **35**, 1168–1178.
41 Q. J. Guan, W. Sun, G. Y. Zhou, J. P. Liu and Z. G. Yin, *Trans. Nonferrous Met. Soc. China*, 2016, **26**, 865–873.
42 T. Guoxin, Z. Yongjun, X. Jingming, Z. Ping, H. Tiandou, X. Yaning and Z. Jing, *Inorg. Chem.*, 2003, **42**, 735–741.
43 S. Khurana, S. Negi and A. Chandra, *Polym. Test.*, 2021, **96**, 107118.
44 P. M. Shanthi, P. J. Hanumantha, T. Albuquerque, B. Gattu and P. N. Kumta, *ACS Appl. Energy Mater.*, 2018, **1**, 483–494.
45 X. Xu, G. Van Eygen, C. Molina-Fernández, D. Nikolaeva, Y. Depasse, S. Chergaoui, Y. Hartanto, B. Van der Bruggen, J. A. Coutinho and A. Buekenhoudt, *J. Membr. Sci.*, 2023, **670**, 121350.